Article

Thermodynamics and Kinetics of PNA–DNA Quadruplex-Forming Chimeras

Luigi Petraccone, Bruno Pagano, Veronica Esposito, Antonio Randazzo, Gennaro Piccialli, Guido Barone, Carlo A. Mattia, and Concetta Giancola

J. Am. Chem. Soc., **2005**, 127 (46), 16215-16223• DOI: 10.1021/ja0545923 • Publication Date (Web): 26 October 2005

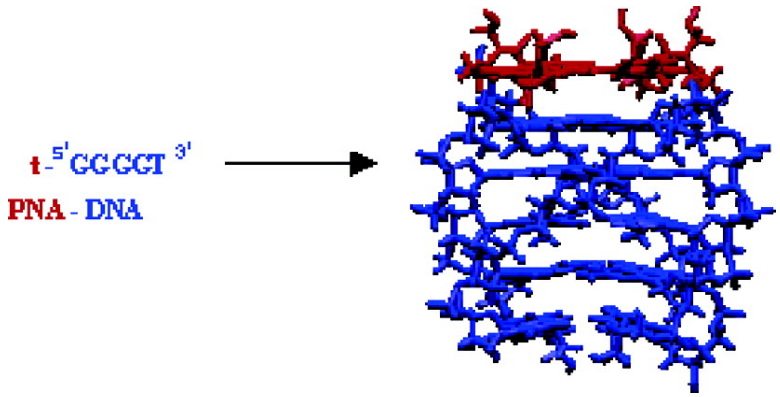

More About This Article

Additional resources and features associated with this article are available within the HTML version:

- Supporting Information
- Links to the 6 articles that cite this article, as of the time of this article download
- Access to high resolution figures
- Links to articles and content related to this article
- Copyright permission to reproduce figures and/or text from this article

View the Full Text HTML

J|A|C|S
ARTICLES
Published on Web 10/26/2005

Thermodynamics and Kinetics of PNA−DNA Quadruplex-Forming Chimeras

Luigi Petraccone,[†] Bruno Pagano,[†] Veronica Esposito,[‡] Antonio Randazzo,[‡] Gennaro Piccialli,[‡] Guido Barone,[§] Carlo A. Mattia,[†] and Concetta Giancola*[,§]

Contribution from the Dipartimento di Scienze Farmaceutiche, Via Ponte Don Melillo, 84084, Fisciano (SA), Italy, Dipartimento di Chimica delle Sostanze Naturali, Via D. Montesano 49, Università "Federico II" di Napoli, 80131, Naples, Italy, and Dipartimento di Chimica, Via Cintia, Università "Federico II" di Napoli, 80126, Naples, Italy

Received July 11, 2005; E-mail: giancola@unina.it

Abstract: PNA−DNA chimeras present the interesting properties of PNA, such as the high binding affinity to complementary single-strand (DNA or RNA), and the resistance to nuclease and protease degradation. At the same time, the limitations of an oligomer containing all PNA residues, such as low water solubility, self-aggregation, and low cellular uptake, are effectively overcome. Further, PNA−DNA chimeras possess interesting biological properties as antisense agents. We have explored the ability of PNA−DNA chimeric strands to assemble in quadruplex structures. The rate constant for association of the quadruplexes and their thermodynamic properties have been determined by CD spectroscopy and differential scanning calorimetry (DSC). Thermal denaturation experiments indicated higher thermal and thermodynamic stabilities for chimeric quadruplexes in comparison with the corresponding unmodified DNA quadruplex. Singular value decomposition analysis (SVD) suggests the presence of kinetically stable intermediate species in the quadruplex formation process. The experimental results have been discussed on the basis of molecular dynamic simulations. The ability of PNA−DNA chimeras to form stable quadruplex structures expands their potential utility as therapeutic agents.

Introduction

It is well-known that guanine-rich oligonucleotides can adopt G-quadruplex structure stabilized by quartet layers of Hoogsteen paired guanine residues.[1] These guanine rich sequences are found at the ends of chromosomes, as telomeric protein complexes, and in a number of biologically significant regions of the genome such as those encoding immunoglobulin switch regions, gene promoter regions, and sequence associated with human diseases.[2−6] G-quadruplexes are also important in the design of novel aptameric nucleic acids as tools aimed at binding and inhibiting particular proteins.[7−9] For example, quadruplex forming oligonucleotides have resulted in being potent inhibitors of HIV-1 integrase, the enzyme responsible for the insertion of viral DNA into the host genome.[10] However, the utilization of aptamers in vivo requires that their properties fit living cell conditions. The chemical modification of oligonucleotides can impart stability to nucleic acids or improve resistance to the enzymatic action of nuclease.[11] One interesting modification is the incorporation of peptide nucleic acid (PNA) units into the canonic nucleic acid backbone leading to PNA−DNA hybrids, the so-called PNA−DNA chimeras.[12,13]

PNAs are oligonucleotide mimics in which the entire sugar−phosphate backbone has been replaced with a pseudopeptide formed by *N*-(2-amino-ethyl)-glycine units, resulting in an achiral and uncharged oligomers (Chart 1).[14] PNA−DNA chimeras present the interesting properties of PNA, such as the high binding affinity to complementary single-strand (DNA or RNA), and the resistance to nuclease and protease degradation. At the same time, the limitations of an oligomer containing all PNA residues, such as low water solubility, self-aggregation, and low cellular uptake, are effectively overcome. Further, PNA−DNA chimeras possess interesting biological properties as antisense agents[15] and also as decoys against NF-kB transcription factors.[16,17] Moreover, PNA−DNA chimeras have

[†] Dipartimento di Scienze Farmaceutiche, Via Ponte Don Melillo.
[‡] Dipartimento di Chimica delle Sostanze Naturali, Università "Federico II" di Napoli.
[§] Dipartimento di Chimica, Università "Federico II" di Napoli.

(1) Phillips, K.; Dauter, Z.; Murchie, A. I. H.; Lilley, D. M. J.; Luisi, B. *J. Mol. Biol.* **1997**, *273*, 171−182.
(2) Blackburn, E. H. *Cell* **1994**, *77*, 621−623.
(3) Sen, D.; Gilbert, W. *Nature* **1988**, *334*, 364−366.
(4) Evans, T.; Schon, E.; Gora-Maslak, G.; Patterson, J.; Efstratiadis, A. *Nucleic Acids Res.* **1984**, *12*, 8043−8058.
(5) Kilpatrick, M. W.; Torri, A.; Kang, D. S.; Engler, J. A.; Wells, R. D. *J. Biol. Chem.* **1986**, *261*, 11350−11354.
(6) Fry, M.; Loebel, L. A. *Proc. Natl. Acad. Sci. U.S.A.* **1994**, *91*, 4950−4954.
(7) Lin, Y.; Padmapriya, A.; Morden, K. M.; Jayasena, S. D. *Proc. Natl. Acad. Sci. U.S.A.* **1995**, *92*, 11044−11048.
(8) Lin, Y.; Jayasena, S. D. *J. Mol. Biol.* **1997**, *271*, 100−111.
(9) Wenn, J.-D.; Gray, D. M. *Biochemistry* **2002**, *41*, 11438−11448.
(10) Jing, N.; Hogan, M. E. *J. Biol. Chem.* **1998**, *273*, 34992−34999.
(11) Kusser, W. *J. Biotechnol.* **2000**, *74*, 27−38 and references therein.
(12) Misra, H. S.; Pandey, P. K.; Modak, M. J.; Vinayak, R.; Pandey, V. N. *Biochemistry* **1998**, *37*, 1917−1925.
(13) Vinayak, R.; Van der Laan, A. C.; Brill, R.; Otteson, K.; Andrus, A.; Kuyl-Yeheskiely, E.; Van Boom, J. H. *Nucleosides Nucleotides* **1997**, *16*, 1653−1656.
(14) Nielsen, P. E.; Egholm, M.; Berg, R. H.; Buchardt, O. *Science* **1991**, *254*, 1497−1500.
(15) van der Laan, A. C.; Havenaar, P.; Oosting, R. S.; Kuyl-Yeheschiely, E. U.; van Boom, J. H. *Bioorg. Med. Chem. Lett.* **1998**, *8*, 663−668.

Chart 1. Structure of PNA, DNA, and DNA/PNA Chimera

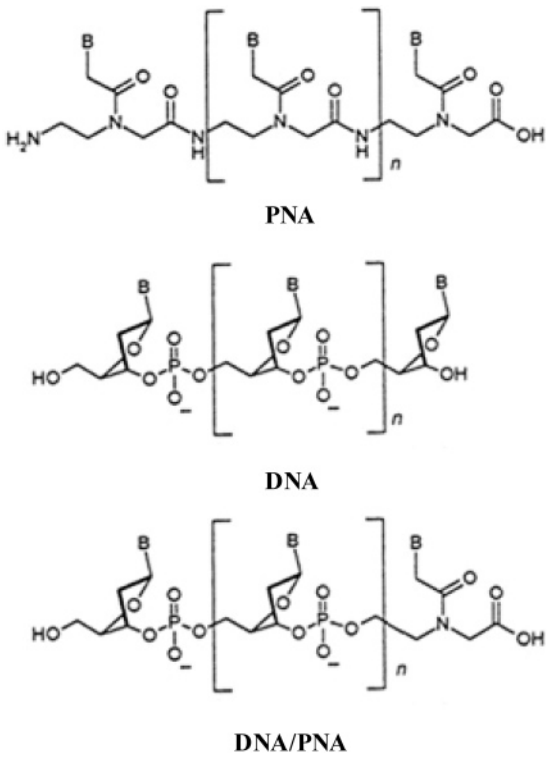

been shown to form triple helix structures becoming a potential drug candidate for antigene therapy and for antisense therapy.[18−20]

In the last years few works appeared in the literature involving PNA or both PNA and DNA in quadruplexes.[21−25] In particular, the formation of two quadruplexes containing all PNA residues[24,25] and a $(PNA)_2$·$(DNA)_2$ hybrid quadruplex has been reported.[22]

We first have shown the ability of PNA−DNA chimeras to form quadruplex structures.[26,27] We found by NMR study that the introduction of a single PNA unit at the 5′ or 3′ end of the $^{5'}$TGGGT$^{3'}$ sequence is optimal for quadruple structure, whereas the $^{5'}$TGG$^{3'}$-gt and tg-$^{5'}$GGT$^{3'}$ (small letters indicate PNA units) sequences did not form well defined structures. This was attributed to the flexibility of the PNA backbone which plays a fundamental role in the unfavorable energetics of quadruplex formation. However, PNA−DNA chimeras with only one PNA unit at 3′ ends are still 25 times more stable in human serum that the corresponding unmodified oligodeoxynucleotides.[28] Therefore, the introduction of a single PNA unit in quadruplex-forming oligonucleotides should enhance the stability against degradation by exonucleases and, hence, the biological activity of these structures involved as active aptamers in a number of quadruplex-binding proteins.[29]

Usually into the development of novel aptamer agents, it is necessary to evaluate the quadruplex stability by thermal denaturation measurements which allows us to obtain the melting temperature (T_m). However, a simple T_m determination does not necessarily reflect the thermodynamic situation at a physiologically relevant temperature. In addition, T_m values could be influenced by a kinetic control of quadruplex assembly. Hence, as argued by Mergny and co-workers, conclusions reached by likening the heating curves to thermodynamic equilibrium curves could be not correct.[30] It is evident that more complete studies are required for a thermodynamic/kinetic description of these systems. In this work we will describe the thermodynamic and kinetic properties of two tetramolecular quadruplexes resulting from the association of four t-$^{5'}$GGGGT$^{3'}$ or four $^{5'}$TGGGG$^{3'}$-t strands (t indicates a thymine PNA unit) in comparison with the thermodynamic and kinetic properties of the parallel DNA quadruplex $[^{5'}TGGGGT^{3'}]_4$, whose structure has been already extensively studied by NMR and X-ray crystallography.[1,31,32]

We will show that it is possible to make equilibrium measurements and to calculate the G-quadruplex stability in terms of ΔG. Spectroscopic (circular dichroism) and calorimetric (differential scanning calorimetry) data will be discussed also on the basis of molecular dynamics calculations. This physicochemical analysis could help to understand the stability of chimeric G-quadruplex and thus to design better therapeutic agents.

Material and Methods

Synthesis and Purification. The chimeras $^{5'}$TGGGG$^{3'}$-t and t-$^{5'}$GGGGT$^{3'}$ were synthesized through a recently proposed solid-phase strategy based on commercially available Bhoc/Fmoc PNA monomers and 3′ or 5′-phosphoramidite nucleosides as building blocks.[26,33] Particularly a Tentagel-OH resin functionalized with a N−Fmoc glycine residue was linked to the first t-PNA unit, and then it was reacted with 5′-O-DMT-3′-O-(2-cyanoethyl)phosphoramidite guanosine and thymidine units to obtain $^{5'}$TGGGG$^{3'}$-t and with 3′-O-DMT-5′-O-(2-cyanoethyl)phosphoramidite guanosine and thymidine units to obtain t-$^{5'}$GGGGT$^{3'}$. The oligomers were detached from the support and deprotected by treatment with concentrated aqueous ammonia at 55 °C for 12 h. The combined filtrates and washings were concentrated under reduced pressure, redissolved in H_2O, and analyzed and purified by HPLC on a Nucleogel SAX column (Macherey-Nagel, 1000-8/46); buffer A: 20 mM KH_2PO_4 aqueous solution, pH 7.0, containing 20% (v/v) CH_3CN; buffer B: 1 M KCl, 20 mM KH_2PO_4 aqueous solution, pH 7.0, containing 20% (v/v) CH_3CN; a linear gradient from 0 to 100% B in 30 min, flow rate 1 mL/min, were used. The isolated oligomers, (retention times: $^{5'}$TGGGG$^{3'}$-t = 16.9 min; t-$^{5'}$GGGGT$^{3'}$ = 17.0 min)

(16) Romanelli, A.; Pedone, C.; Saviano, M.; Bianchi, N.; Borgatti, M.; Mischiati, C.; Gambari, R. *Eur. J. Biochem.* **2001**, *268*, 6066−6075.
(17) Borgatti, B.; Breda, L.; Cortesi, R.; Nastruzzi, C.; Romanelli, A.; Saviano, M.; Bianchi, N.; Mischiati, C.; Pedone, C.; Gambari, R. *Biochem. Pharmacol.* **2002**, *64*, 609−616.
(18) Barawkar, D. A.; Kwok, Y.; Bruice, T. W.; Bruice, T. C. *J. Am. Chem. Soc.* **2000**, *122*, 5244-5250.
(19) Ferrer, E.; Shevchenko, A.; Eritja, R. *Bioorg. Med. Chem.* **2000**, *8*, 291−297.
(20) Petraccone, L.; Erra, E.; Messere, A.; Montesarchio, D.; Piccialli, G.; De Napoli, L.; Barone, G.; Giancola, C. *Biopolymers* **2004**, *73*, 434−442.
(21) Datta, B.; Armitage, B. A. *J. Am. Chem. Soc.* **2001**, *123*, 9612−9612.
(22) Datta, B.; Schmitt, C.; Armitage, B. A. *J. Am. Chem. Soc.* **2003**, *125*, 4111−4118.
(23) Green, J. J.; Ying, L.; Klenerman, D.; Balasubramanian, S. *J. Am. Chem. Soc.* **2003**, *125*, 3763−3767.
(24) Krishnan-Ghosh, Y.; Stephens, E.; Balasubramanian, S. *J. Am. Chem. Soc.* **2004**, *126*, 5944−5945.
(25) Datta, B.; Bier, M. E.; Roy, S.; Armitage, B. A. *J. Am. Chem. Soc.* **2005**, *127*, 4199−4207.
(26) Esposito, V.; Randazzo, A.; Messere, A.; Galeone, A.; Petraccone, L.; Giancola, C.; Piccialli, G.; Mayol, L. *Eur. J. Org. Chem.* **2003**, *17*, 3364−3371.
(27) Esposito, V.; Galeone, A.; Mayol, L.; Messere, A.; Piccialli, G.; Randazzo, A. *Nucleosides Nucleotides Nucleic Acids* **2003**, *22*, 1681−1684.
(28) Bergmann, F.; Bannwarth, W.; Tam, S. *Tetrahedron Lett.* **1995**, *36*, 6823−6826.
(29) Shafer, R. H.; Smirnov, I. *Biopolymers* **2001**, *56*, 209−227.
(30) Mergny, J. L.; De Cian, A.; Ghelab, A.; Sacca, B.; Lacroix, L. *Nucleic Acids Res.* **2005**, *33*, 81−94.
(31) Laughlan, G.; Murchie, A. I. H.; Noman, D. G.; Moore, M. H.; Moody, P. C. E.; Lilley, D. M. J.; Luisi, B. *Science* **1994**, *265*, 520−524.
(32) Aboul-ela, F.; Murchie, A. I. H.; Norman, D. G.; Lilley, D. M. J. *J. Mol. Biol.* **1994**, *243*, 458−471.
(33) Capasso, D.; De Napoli, L.; Di Fabio, G.; Messere, A.; Montesarchio, D.; Pedone, C.; Piccialli, G.; Saviano, M. *Tetrahedron* **2001**, *57*, 9481−9846.

were collected and successively desalted by Sep-Pak columns (C18). The isolated oligomers were desalted and analyzed by MALDI-TOF mass spectrometry and ^{1}H NMR. They resulted in being more than 97% pure.

Preparation of Quadruple Helices. DNA quadruplexes were formed by dissolving solid lyophilized oligonucleotide in the appropriate buffer and were annealed by heating to 90 °C for 5 min and slow cooling to room temperature. The buffer used was 10 mM sodium phosphate, 200 mM NaCl, 0.1 mM EDTA at pH = 7.0. The $^{5'}$TGGGGT$^{3'}$, t-$^{5'}$GGGGT$^{3'}$, and $^{5'}$TGGGG$^{3'}$-t concentrations were determined by their adsorption measured at 90 °C, in the same buffer, using as molar extinction coefficient ϵ(260 nm) = 57 800 M^{-1} cm^{-1}. The molar extinction coefficients were calculated by the nearest neighbor model,[34] assuming that the extinction coefficient of the nucleobases in the DNA−PNA chimeras was the same as in DNA.

DSC Experiments. Differential scanning calorimetry (DSC) measurements were carried out on a second generation Setaram Micro-DSC. The experiments were performed at constant single strand concentration of 6.6×10^{-4} M. The apparent molar heat capacity vs temperature profiles were obtained at different scan rates (see Supporting Information Figure S1). The excess heat capacity function $\langle \Delta C_P \rangle$ was obtained after baseline subtraction, assuming that the baseline is given by the linear temperature dependence of the native state heat capacity.[35] No baseline difference was observed before and after the transition indicating a negligible heat capacity difference between the initial and final states. The transition enthalpies, ΔH°_{cal} were obtained by integrating the area under the heat capacity versus temperature curves. With decreasing heating rate, the melting temperature changes, indicating nonequilibrium conditions. Equilibrium melting curves were obtained by CD experiments (see next section).

CD Melting Experiments. CD spectra of the quadruplexes were registered on a Jasco 715 circular dichroism spectrophotometer in a 0.1 cm path length cuvette. The wavelength was varied from 220 to 340 nm at 5 nm min^{-1}. The spectra were recorded with a response of 16 s, at 2.0 nm bandwidth and normalized by subtraction of the background scan with buffer. The molar ellipticity was calculated from the equation $[\vartheta] = 100\vartheta/cl$ where ϑ is the relative intensity, c is the single strand concentration (4×10^{-5} M), and l is the path length of the cell in centimeters.

The equilibrium melting curves for all the quadruplexes were obtained by collecting data in the range 10−70 °C using a temperature step of 5 °C. The samples were incubated at each temperature for a suitable time to achieve the equilibrium before recording the CD. Reaching equilibrium at each temperature was guaranteed by the achievement of superimposable CD spectra on changing time. The equilibrium was generally obtained within few hours at highest temperatures (>50 °C), but much longer times (some days) were needed for the lowest temperatures (<30 °C). The melting curves were obtained reporting the CD signal at 264 nm as a function of temperature. The CD melting curves were analyzed by using standard procedures reported by Marky and Breslauer and correspond to a two-state approximation of the helix−coil transition of each molecule.[36] The T_m and $\Delta H^\circ_{V.H.}$ values reported in Table 1 provide the best fit of the experimental meltingdata.The reported errors for thermodynamic parameters are the standard deviations of the mean from the multiple determinations.

The values of the free energy change at 298 K were calculated from $\Delta G^\circ = -RT \ln K(298)$ where the equilibrium constant at 298 K was evaluated by means of the van't Hoff equation:

$$\ln\left[\frac{K(T_m)}{K(298)}\right] = \frac{\Delta H^\circ}{R}\left(\frac{1}{298} - \frac{1}{T_m}\right)$$

where we assumed that the fraction of single strand in quadruplex is 0.5 at T_m and the value of $K(T_m)$ is 32 C_Q^3 (C_Q = total quadruplex concentration) and that the difference in heat capacity between the initial and final states is negligible. Indeed, no significant ΔC_p was observed as already found by different authors.[37−40] The ΔS° values at 298 K were calculated by the equation $\Delta S^\circ = (\Delta H^\circ - \Delta G^\circ)/298$.

Kinetic Experiments. Association of single strands into quadruplex structure was monitored for each sequence in the same buffer used for the melting experiments. All the experiments were performed at two different concentrations of single strand: 4×10^{-5} M and 2×10^{-4} M. The samples were incubated in a bath at 90 °C for 5 min to dissociate any tetramer. The structural transition from the single strands to the tetramolecular quadruplex was monitored at 20 °C by recording the CD spectra as a function of time. Assuming that dissociation is negligible, the single strand concentration at any time is given by

$$[S]_t^{1-n} - [S]_0^{1-n} = 4(n-1)kt \quad (1)$$

where $[S]_t$ is the single strand concentration at time t, $[S]_0$ is the initial single strand concentration, n is the order of the reaction with respect to the single strand concentration, and k is the rate constant for disappearance of single strands. The changes in CD spectra are directly proportional to $[S]_0$ and $[S]_t$ according to the following equations:

$$\Theta_\infty - \Theta_0 = \alpha[S]_0 \quad (2)$$

$$\Theta_\infty - \Theta_t = \alpha[S]_t \quad (3)$$

where Θ_∞ and Θ_0 correspond to the ellipticity of the final and initial state, respectively. Θ_t is the ellipticity at time t. By substituting eqs 2 and 3 in eq 1, the following was obtained:

$$(\Theta_\infty - \Theta_t)^{1-n} - (\Theta_\infty - \Theta_0)^{1-n} = 4(n-1)\alpha^{1-n}kt \quad (4)$$

defining $k' = 4\alpha^{1-n}k$ the eq 4 can be rewritten as

$$\Theta_t = \Theta_\infty - [(\Theta_\infty - \Theta_0)^{1-n} + (n-1)k't]^{1/1-n} \quad (5)$$

The association rate constants and the reaction orders were obtained by fitting the ellipticity at 264 nm as a function of time by means of eq 5 using the GNUPLOT 3.7 software. The $t_{1/2}$ values were calculated by the equation $t_{1/2} = 7/3k[S]_0^3$.

Singular Value Decomposition Analysis. The CD spectra versus temperature and versus time were analyzed by singular value decomposition (SVD) to determine the number of significant spectral species involved in the equilibrium melting and kinetic experiments.[41−43] All SVD calculations were performed using the program developed by Konno.[44] The matrix of the CD spectra A is decomposed by the SVD method into the product of three matrices:

$$A = USV^t$$

The matrix U contains the basis spectra, S is a diagonal matrix that contains the singular values, and V is a matrix containing the coefficient vectors. Examination of the autocorrelation functions of the basis spectra

(34) Cantor, C. R.; Warshow, M. M.; Shapiro, H. *Biopolymers* **1970**, *9*, 1059−1077.
(35) Freire, E.; Biltonen, R. L. *Biopolymers* **1978**, *17*, 463−479.
(36) Marky, L. A.; Breslauer, K. J. *Biopolymers* **1987**, *26*, 1601−1620.
(37) Lu, M.; Guo, Q.; Kallenbach, N. R. *Biochemistry* **1993**, *32*, 598−601.
(38) Kankia, B. I.; Marky, L. A. *J. Am. Chem. Soc.* **2001**, *123*, 10799−10804.
(39) Ren, J.; Qu, X.; Trent, J. O.; Chaires, J. B. *Nucleic Acids Res.* **2002**, *30*, 2307−2315.
(40) Risitano, A.; Fox, K. R. *Nucleic Acids Res.* **2004**, *32*, 2598−2606.
(41) Henry, R. W.; Hofrichter, J. *Methods Enzymol.* **1992**, *210*, 129−192.
(42) Hendler, R. W.; Shrager, R. I. *J. Biochem. Biophys. Methods* **1994**, *28*, 1−33.
(43) Haq, I.; Chowdhry, B. Z.; Chaires, J. B. *Eur. Biophys. J.* **1997**, *26*, 419−426.
(44) Konno, T. *Protein Sci.* **1998**, *7*, 975−982.

and the coefficient vectors permits us to determine the minimum number of component spectra required to describe the data within the random noise. The value of the autocorrelation function is a measure of the smoothness between adjacent row elements. Values near 1 indicate slow variation from row to row or "signal". A value of the autocorrelation function higher than 0.6 for both the *U* and *V* matrices was selected as a cutoff criterion for accepting a significant spectral species.

Molecular Modeling. The initial structure of the $[^{5'}TGGGGT^{3'}]_4$ quadruplex was generated by using the coordinates of the previously reported structure.[31] The chimeric quadruplexes $[t\text{-}^{5'}GGGGT^{3'}]_4$ and $[^{5'}TGGGG^{3'}\text{-}t]_4$ were generated from the DNA quadruplex replacing the dT residue at the 5′-end and at the 3′-end, respectively, with the corresponding PNA unit. Particularly, the 5′-phosphate or 3′-phosphate moiety of the oligonucleotide fragment in the chimera was linked to the NH_2 group of the PNA unit through a phosphoramidate bond, and then the C-terminal of PNA was linked, via an amide bond, to a glycine residue. New parameters for the phosphoramidate bond and for the PNA units were added to the standard Amber force field.[45] The stretch, bend, and torsion force constants were assigned to the N−P group by analogy with phosphate constants in the Amber force field. The bond stretch force constants for NQ-P and CT-NQ (NQ is the type of nitrogen atom in the phosphoramidate bond) were set slightly higher than those in the unmodified backbone in order to model the possible conjugation in the N−P group using the parameters reported by Ding and co-workers.[46] To describe the PNA part of the strands the parameters and atomic charges reported by Shields and co-workers[47] were used. The resulting coordinates of the chimeric quadruplexes were energy-minimized in a vacuum for 200 steps of the steepest descent method keeping the DNA residues fixed in position allowing only the PNA units to relax. Three internal sodium ions were positioned in the central channel to allow coordination, for each sodium ion, with the four carbonyl oxygen atoms of the two adjacent G-quartets completing the octahedral coordination sphere. The remaining sodium counterions were placed into the most negative locations using the Coulombic potential term with the LEAP module of the AMBER 7.0 package.[48,49] All cations were considered as part of the solvent including those in the channel. Then, each quadruplex was surrounded by a periodic box TIP3P water[50] extended to a distance of 10 Å from any solute atom.

Calculations were performed using the SANDER module of the AMBER 7.0 package with SHAKE on the hydrogen atoms with a tolerance of 0.000 01 Å and a 2 fs time step. The particle mesh Ewald method (PME) within AMBER 7 was used for the calculation of electrostatic interactions. Initial systems were energy minimized using 1000 steps of the steepest descent method followed by the conjugate method until convergence to an rms gradient of 0.1 kcal mol^{-1} $Å^{-1}$.

To equilibrate the solvent molecules, all the waters and surrounding counterions were subjected to 15 ps dynamics at 200 K, keeping DNA and PNA residues fixed, followed by an energy minimization of the entire system. The quenched systems were then heated slowly from 0 to 300 K by coupling to a heat bath over a period of 25 ps after which the MD simulations were continued (for 4.5 ns) at constant temperature (300 K) and pressure (1 bar) using the Berendsen algorithm[51] with a coupling constant of 0.2 ps, snapshots were collected every 1 ps. The MD trajectories were analyzed using the ptraj and carnal modules of the AMBER 7.0 package.

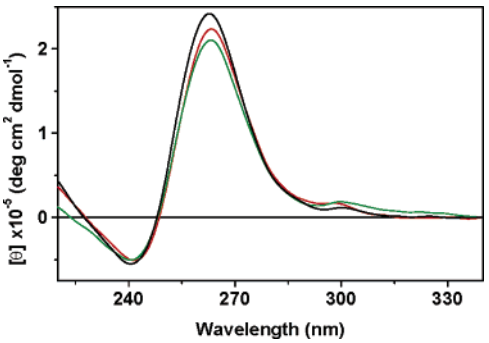

Figure 1. CD spectra of $^{5'}TGGGGT^{3'}$ (red) $^{5'}TGGGG^{3'}$-t (black) and $t\text{-}^{5'}GGGGT^{3'}$ (green). Data were collected at 4×10^{-5} M single strand concentration at 20 °C. All measurements were carried out in buffers consisting of 10 mM sodium phosphate, 200 mM NaCl, 0.1 mM EDTA at pH = 7.0.

Result and Discussion

Thermodynamics of Quadruplex Dissociation. The dissociation of the quadruplexes was investigated using microcalorimetry and circular dichroism techniques. The CD spectra of the chimeric sequences are quite similar to the spectrum of the unmodified counterpart and are characterized by a positive band at 264 nm and a negative band at 243 nm (Figure 1). These spectra are characteristic of parallel-stranded quadruplex structures.[52,53] The differences in the intensity of the positive band at 264 nm indicate slight structural/conformational differences in the three quadruplexes.

To further confirm the parallel arrangement of the strands in the chimeric quadruplexes, 1D ^1H NMR spectra of $^{5'}TGGGG^{3'}$-t and $t\text{-}^{5'}GGGGT^{3'}$ were acquired. Both spectra show only six signals in the aromatic region (where the PNA bases' proton signals are upfield shifted in comparison to those of the corresponding DNA residues) and three well-defined singlets in the region 11−12 ppm. In analogy to $^{5'}TGGGGT^{3'}$, the number of the observed signals suggests the formation of 4-fold symmetric G-quadruplexes with all strands parallel to each other and containing four G-tetrads.[32]

The melting temperatures and the calorimetric profiles for each system were influenced by scan rate (Figure 2). This arises when the complexes are not at thermodynamic equilibrium during the temperature changes and it is due to slow rates of dissociation and/or association process.[30,52] Consequently, the thermodynamic parameters cannot be obtained from DSC melting experiments, and the calorimetric T_m values should be considered an upper limit. In these nonequilibrium conditions, only the enthalpy change relative to the quadruplex dissociation process may be directly obtained by differential scanning microcalorimetry measurements.

To perform a complete thermodynamic analysis, the equilibrium melting curves for all the quadruplexes were obtained

Table 1. Thermodynamic Parameters for the Dissociation of the Quadruplexes

quadruplex	T_m (°C)	ΔH°_{cal} (kJ mol^{-1})	$\Delta H^\circ_{V.H.}$ (kJ mol^{-1})	ΔS° (kJ mol^{-1} K^{-1})	ΔG°_{298} (kJ mol^{-1})
$[^{5'}TGGGGT^{3'}]_4$	37 ± 1	320 ± 10	325 ± 13	0.79 ± 0.04	90 ± 1
$[^{5'}TGGGG^{3'}\text{-}t]_4$	41 ± 1	312 ± 10	323 ± 12	0.77 ± 0.03	93 ± 1
$[t\text{-}^{5'}GGGGT^{3'}]_4$	44 ± 1	352 ± 13	360 ± 15	0.88 ± 0.04	98 ± 2

(45) Cornell, W. D.; Cieplack, P.; Bayly, C. I.; Gould, I. R.; Merz, K. M.; Ferguson, D. M.; Spellmeyer, D. C.; Fox, T.; Caldwell, J. W.; Kollman, P. A. *J. Am. Chem. Soc.* **1995**, *117*, 5179−5197.
(46) Ding, D.; Gryaznov, S. M.; Wilson, D. W. *Biochemistry* **1998**, *37*, 12082−12093.
(47) Shields, G. C.; Laughton, C. A.; Orozco, M. *J. Am. Chem. Soc.* **1998**, *120*, 5895−5904.
(48) Kollman, P. A. et al. *AMBER 7*; University of California: San Francisco, CA, 2002.
(49) Case, D. A.; Pearlman, D. A.; Caldwell, J. W.; Ross, W. S.; Cheatham, T. E., III; DeBolt, S.; Ferguson, D.; Seibel, G.; Kollman. P. *Comput. Phys. Commun.* **1995**, *91*, 1−41.
(50) Jorgensen, W. L.; Chandrasekhar, J.; Madura, J. D.; Impey, R. W.; Klein, M. L. *J. Chem. Phys.* **1983**, *79*, 926−935.
(51) Berendsen, H. J. C.; Postma, J. P. M.; van Gunsteren, W. F.; Dinola, A.; Haak, J. R. *J. Chem. Phys.* **1984**, *81*, 3684−3690.

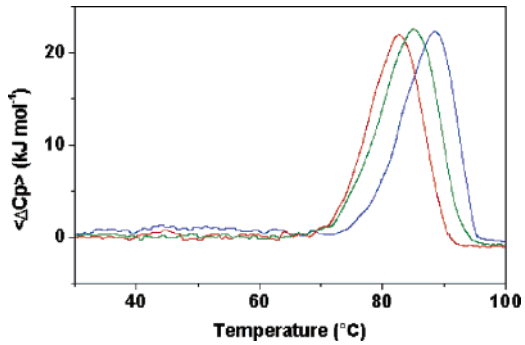

Figure 2. Calorimetric heat capacity versus temperature profiles for $^{5'}$TGGGG$^{3'}$-t sequence at scan rate of 1.0 °C/min (blue), 0.5 °C/min (green), and 0.3 °C/min (red). Data were collected at 6.6×10^{-4} M single strand concentration. All measurements were carried out in buffers consisting of 10 mM sodium phosphate, 200 mM NaCl, 0.1 mM EDTA at pH = 7.0.

by collecting CD data in the range 10−70 °C using a temperature step of 5 °C. The samples were equilibrated at each temperature for a suitable time before recording the CD signal. The spectra of the quadruplexes as a function of temperature are shown in Figure 3. As the temperature increases, the negative band at 243 nm and the positive band at 264 nm are reduced in magnitude and shifted to lower wavelengths. The molar ellipticity at 264 nm represents a zero ellipticity point in the spectrum of the single strand. Consequently, the molar ellipticity at 264 nm gives a reasonably accurate assessment of the change in quadruplex population upon association or dissociation.[54] The molar ellipticity at 264 nm was reported as a function of temperature for all the studied quadruplexes, and the resulting curves represent the equilibrium melting curves (Figure 3). The melting temperatures and van't Hoff enthalpy change values were derived by computer fitting of CD melting curves assuming a two-state process. These values are listed in Table 1 along with calorimetric enthalpies. The close correspondence between the calorimetric and van't Hoff enthalpies is consistent with a two-state equilibrium in which intermediate states are not significantly populated and indicates that no aggregation phenomenon occurs during the transition.

Inspection of thermodynamic data reveals that both the chimeric quadruplexes are more stable than [$^{5'}$TGGGGT$^{3'}$]$_4$, [t-$^{5'}$GGGGT$^{3'}$]$_4$ being the most stable one. Particularly, the introduction of a PNA unit at the 5′-end or 3′-end of the $^{5'}$TGGGGT$^{3'}$ sequence increases the T_m value of 7 °C and 4 °C, respectively. The enthalpy value for the unmodified DNA quadruplex is in agreement with the value previously reported for the same quadruplex.[30,55] The $\Delta H°$ values for the chimeric [$^{5'}$TGGGG$^{3'}$-t]$_4$ quadruplex and the DNA quadruplex are quite similar, whereas the enthalpy value for the [t-$^{5'}$GGGGT$^{3'}$]$_4$ quadruplex results in being 35 kJ mol^{-1} higher. These results suggest that the PNA units at the 5′-end, but not at 3′-end, efficiently participate in the interstrand interactions.

To test the two-state approximation for the melting of the studied quadruplexes, the SVD analysis of the wavelength versus temperature matrices was performed. The first 10 singular values obtained for each system with the corresponding autocorrelation functions of the basis spectra (columns of *U*) and the coefficient vectors (columns of *V*) are reported in Table 2. Inspection of Table 2 reveals that, over the entire temperature range investigated, the CD spectra are well described by two basis spectra, as demonstrated by the values of the first-order autocorrelation function (a value higher than 0.6 for both the *U* and *V* matrices was selected as a cutoff criterion for accepting a significant spectral species). The contributions of all of the remaining basis spectra are within the noise. These observations suggest that, for our systems, the quadruplex to single strand transition involves only two significant spectral species.

Modeling. All the simulations were found to be quite stable as noted in macroscopic properties of the systems such as potential and total energy, the density, etc. (data not shown). All-parallel guanine quadruplex stems, including the monovalent cations in the central channel, are rigid and very stable as demonstrated by the time evolution of RMSD values of the dG residues with respect to the starting structure: the average values remain in the range 1.3−1.7 Å (Figure 4a).

To explore the dynamic properties of the PNA regions, the RMSD values were calculated for the atoms of the PNA units of the chimeric quadruplexes. Figure 4b represents the comparison between the time dependence of the RMSD values for the PNA units at 3′ and 5′-end. It is clearly seen that the RMSD has reached a steady average value (3.0 Å) for the PNA units of the [t-$^{5'}$GGGGT$^{3'}$]$_4$ quadruplex whereas it increases after the first 1.5 ns of dynamic for the PNA units of the [$^{5'}$TGGGG$^{3'}$-t] quadruplex.

These results can be correlated with the different dynamics of the PNA units in the two chimeric quadruplexes. Indeed, visual inspection of the trajectories reveals a local unfolding of the 3′-end PNA units on a nanosecond time scale in agreement with the corresponding increase of the observed RMSD value. Particularly, at the end of the simulation, three 3′-PNA units project away from the helical axis of the quadruplex and do not participate in the quadruplex motif. On the other hand, the PNA units of the [t-$^{5'}$GGGGT$^{3'}$]$_4$ quadruplex reach a stable conformation after 300 ps of simulation and remain structured during all the simulation. Particularly, two stable T−T base pairs were observed with N3(T)−O6(T) H-bond distances < 3.5 Å for more than 50% of the dynamic time (Figure 5).

The average structures of the studied quadruplexes, over the last 0.6 ns of MD trajectories, are shown in Figure 6. It can be noted that three 3′-PNA units are completely opened, whereas all the thymines of the 5′-PNA units remain coplanar and parallel to the adjacent G-tetrad maintaining the stacking interactions. The base-pairing interactions between the thymine bases of the 5′-PNA units and the stacking interactions between the thymine bases and the adjacent guanines may justify the higher enthalpy change observed for the dissociation of the [t-$^{5'}$GGGGT$^{3'}$]$_4$ quadruplex in comparison with both the [$^{5'}$TGGGG$^{3'}$-t] and [$^{5'}$TGGGGT$^{3'}$] quadruplexes.

The different behavior of the PNA units in the two chimeric quadruplexes is well summarized by the residue fluctuations reported in Figure 7. The largest fluctuations are associated with the 3′-PNA units of the [$^{5'}$TGGGG$^{3'}$-t] quadruplex, whereas in the [t-$^{5'}$GGGGT$^{3'}$]$_4$ quadruplex the fluctuations of the PNA units have the same magnitude of the fluctuations of the corresponding dT residues of the DNA quadruplex. The slower mobility

(52) Wyatt, R. J.; Davis, P. W.; Freier, S. M. *Biochemistry* **1996**, *35*, 8002−8008.
(53) Petraccone, L.; Erra, E.; Nasti, L.; Galeone, A.; Randazzo, A.; Mayol, L.; Barone, G.; Giancola, C. *Int. J. Biol. Macromol.* **2002**, *31*, 131−137.
(54) Hardin, C. C.; Corregan, M. J.; Lieberman, D. V.; Brown, B. A., II. *Biochemistry* **1997**, *36*, 15428−15450.
(55) Petraccone, L.; Erra, E.; Esposito, V.; Randazzo, A.; Mayol, L.; Nasti, L.; Barone, G.; Giancola, C. *Biochemistry* **2004**, *43*, 4877−4884.

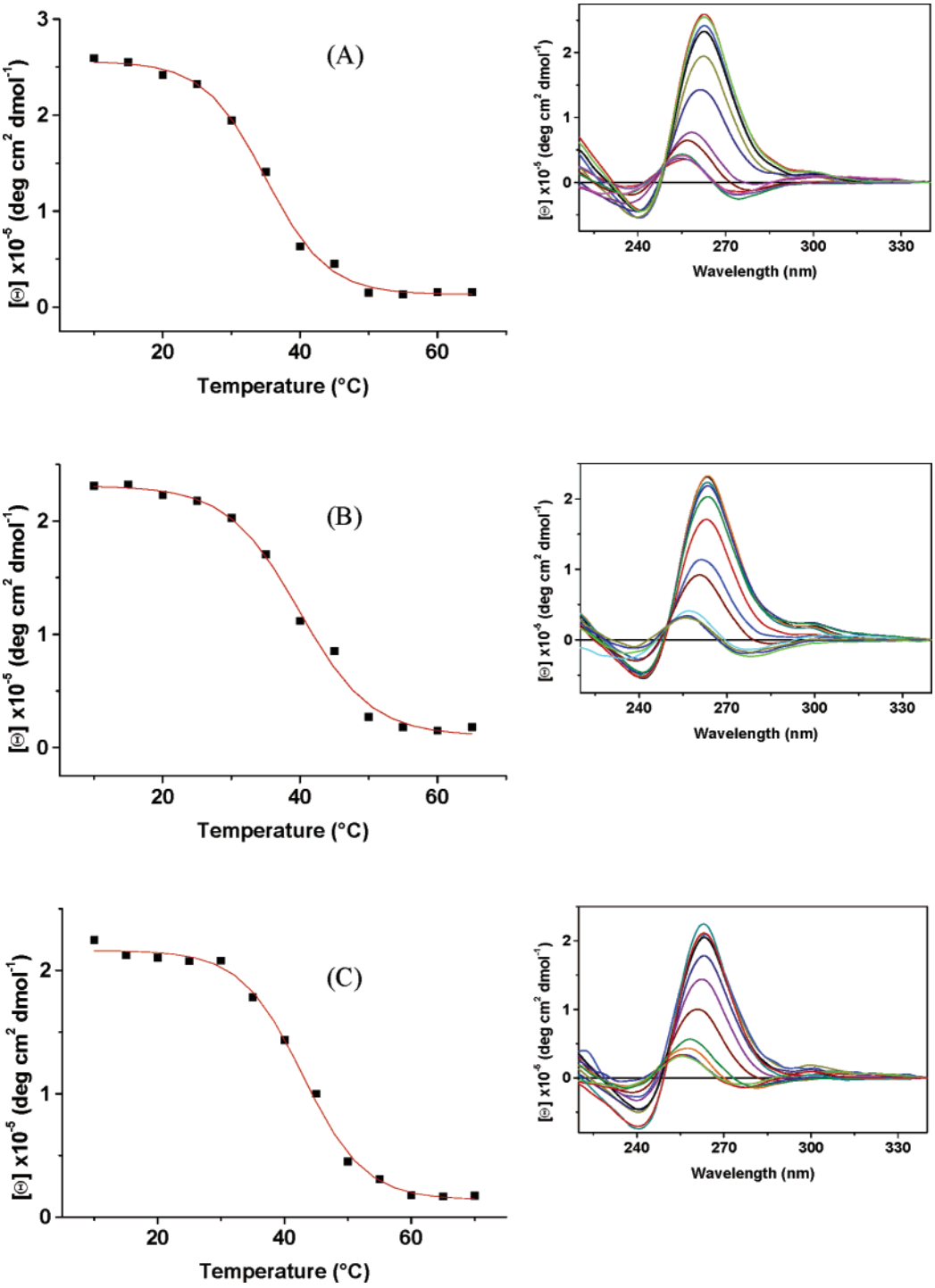

Figure 3. Molar ellipticity at 264 nm as a function of temperature for $^{5'}$TGGGGT$^{3'}$ (A), $^{5'}$TGGGG$^{3'}$-t (B), and t-$^{5'}$GGGGT$^{3'}$ (C) (on the left) with the corresponding CD spectra at different temperatures (on the right).

of the 5′-PNA units in comparison to the 3′-PNA units suggests that the [t-$^{5'}$GGGGT$^{3'}$]$_4$ quadruplex possesses a more rigid structure with a lower entropy. This could justify the major entropic gain observed for the dissociation process of this quadruplex in comparison with the [$^{5'}$TGGGG$^{3'}$-t)] quadruplex.

All these findings indicate that the introduction of the same PNA unit can produce different effects according to whether 5′ or 3′ ends are involved. This could be explained by the asymmetry of the quadruplex ends due to the polarity and the parallel orientation of the strands. Indeed, the 3′-PNA and 5′-PNA units have different local environments and may have different inter- and intrastrand interactions.

Kinetic Study. The kinetics of quadruplex formation was studied by monitoring the ellipticity at 264 nm as a function of time after heating the sample at 90 °C for 5 min and fast cooling to 20 °C.

The experimental curves were fit by means of eq 5 (see Material and Methods Kinetic Experiments section). In Figure 8 the ellipticity vs time at 20 °C is shown for the [$^{5'}$TGGGGT$^{3'}$]$_4$ quadruplex.

Table 2. Results from Singular Value Decomposition of Quadruplex Melting Data

		autocorrelation	
quadruplex	singular values	U matrix	V matrix
$[^{5'}TGGGGT^{3'}]_4$	214.299	0.9994	0.8319
	35.743	0.9986	0.7859
	32.240	0.9987	−0.1384
	12.073	0.9871	−0.1012
	2.609	0.9439	0.1421
	2.110	0.8815	0.0114
	1.964	0.8835	−0.0806
	1.847	0.8936	−0.2465
	1.782	0.8752	−0.5266
	1.637	0.8461	−0.1602
$[^{5'}TGGGG^{3'}\text{-t}]_4$	217.542	0.9996	0.8933
	30.430	0.9980	0.7873
	18.911	0.9981	−0.1761
	9.483	0.9827	0.1406
	2.552	0.9229	0.1474
	2.173	0.9063	−0.0446
	2.053	0.8932	−0.2182
	1.988	0.8871	−0.2793
	1.821	0.8629	−0.0582
	1.673	0.8480	−0.3039
$[\text{t-}^{5'}GGGGT^{3'}]_4$	189.266	0.9996	0.8715
	27.609	0.9983	0.6024
	26.806	0.9966	0.5281
	9.454	0.9624	−0.2198
	4.374	0.9272	−0.1110
	2.552	0.9224	−0.1725
	2.123	0.8879	−0.1518
	1.898	0.8679	0.2052
	1.858	0.8775	−0.1230
	1.571	0.8575	−0.2184

All the data were well fitted by reaction order of 4.0. The same reaction order was obtained at 4×10^{-5} M single strand concentration. The kinetic parameters for all the studied systems are summarized in Table 3. Inspection of the rate constants and $t_{1/2}$ values reveals that the chimeric strands assemble more slowly than the DNA strands. The fourth-order rate constant at 20 °C was $(3.0 \pm 0.2) \times 10^7$ for the $[^{5'}TGGGGT^{3'}]_4$ quadruplex and $(2.1 \pm 0.2) \times 10^7$ for both the chimeric quadruplexes. The rate constant obtained for the DNA quadruplex is consistent with the Arrhenius plots reported for the same quadruplex by Mergny and co-workers.[30]

Our data are in agreement with the mechanism for tetramer formation reported by Wyatt and co-workers.[52] These authors proposed the following mechanism:

$$4\,S \underset{\text{fast equilibrium}}{\longleftrightarrow} 2\,D \underset{k_{-2}}{\overset{k_2}{\rightleftharpoons}} Q$$

where single strands (S) and dimers (D) are in rapid pre-equilibrium that favors single strand and the quadruplex formation from dimer is rate limiting. This mechanism is consistent with the observed fourth-order dependence of the association rate on the concentration of single strand and does not require an improbable four-body collision. Further, the CD spectra vs time do not show an isoelliptic point indicating that could be present intermediate species (see Supporting Information Figure S2). To better explore the formation mechanism of the studied quadruplexes, singular value decomposition analysis of the wavelength versus time matrices was performed. Analysis of the autocorrelation function (Table 4), for both *U* and *V* matrices, suggests that three significant spectral species must be considered to account for the CD spectra obtained by the kinetic experiments on the chimeric quadruplexes, whereas only two spectral species are needed for the DNA quadruplex.

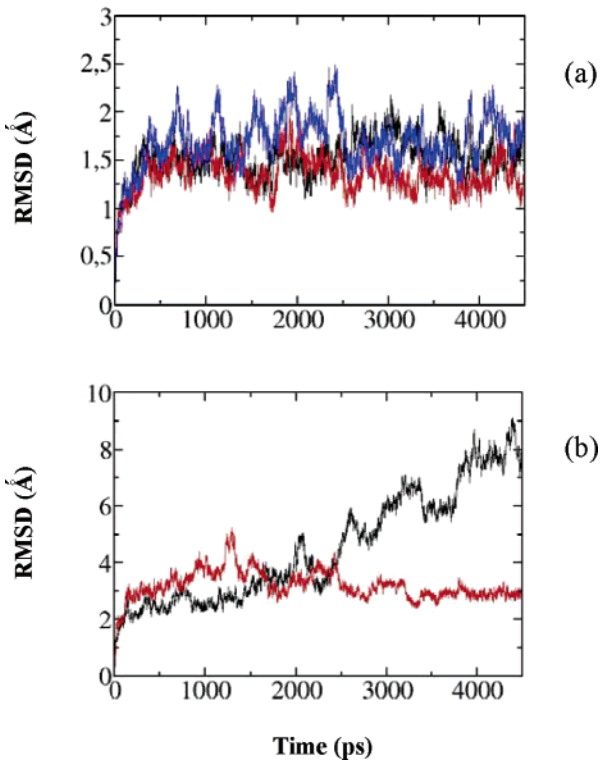

Figure 4. (a) Evolution of the RMSD value of the dG residues for the different quadruplexes with respect to their starting structures, $[^{5'}TGGGGT^{3'}]_4$ (black), $[^{5'}TGGGG^{3'}\text{-t}]_4$ (blue), and $[\text{t-}^{5'}GGGGT^{3'}]_4$ (red). (b) Comparison of the time evolution of the RMSD of the 5′-PNA (red) and 3′-PNA (black) units with respect to their starting structures.

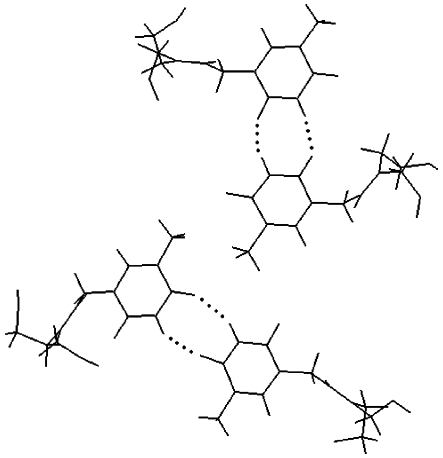

Figure 5. Interstrand T−T base pairs formed by the thymine bases of the 5′-PNA units in the $[\text{t-}^{5'}GGGGT^{3'}]_4$ quadruplex.

It can be noted that SVD analysis gives different responses when applied to equilibrium melting or kinetic data in the case of the chimeric quadruplexes. To visualize these results, in Figure 9 are compared the coefficient vectors v_1-v_4 obtained by the SVD analysis on the kinetic and melting CD spectra for the $[^{5'}TGGGG^{3'}\text{-t}]_4$ quadruplex. Signal-to-noise ratios of v vectors are excellent only for the first two components derived by the melting data, whereas three components must be considered when analyzing the data sets derived by kinetic experiments (similar results was obtained for the $[\text{t-}^{5'}GGGGT^{3'}]_4$

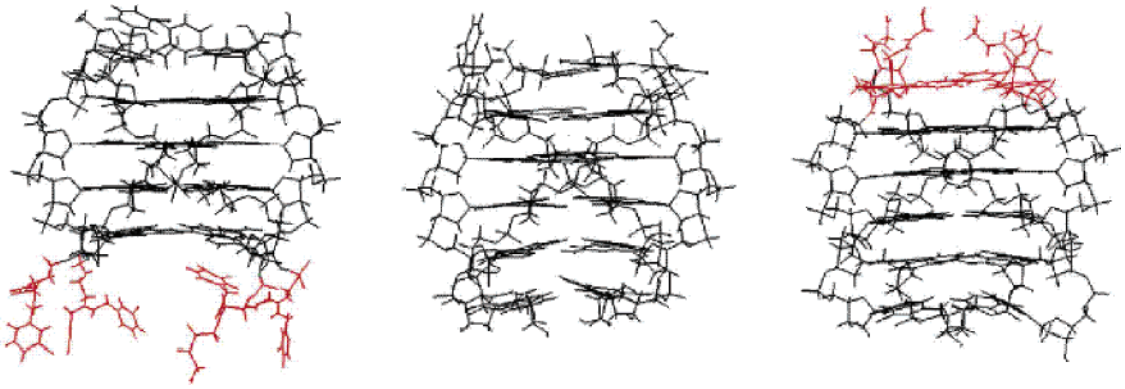

Figure 6. MD average quadruplex structures obtained during the last 0.6 ns of simulation; [5′TGGGG3′-t]$_4$ (on the left), [5′TGGGGT3′]$_4$ (in the middle), [t-5′GGGGT3′]$_4$ (on the right). The PNA units are shown in red.

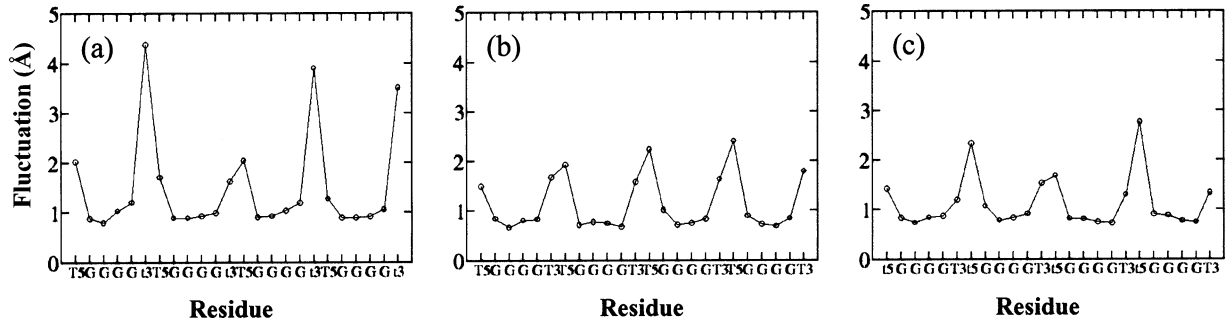

Figure 7. Residues fluctuations of the [5′TGGGG3′-t]$_4$ (a), [5′TGGGGT3′]$_4$ (b), and [t-5′GGGGT3′]$_4$ (c). T5 and T3 represent the dT residue at the 5′-end and 3′-end, respectively (the small letter t indicates the corresponding PNA unit).

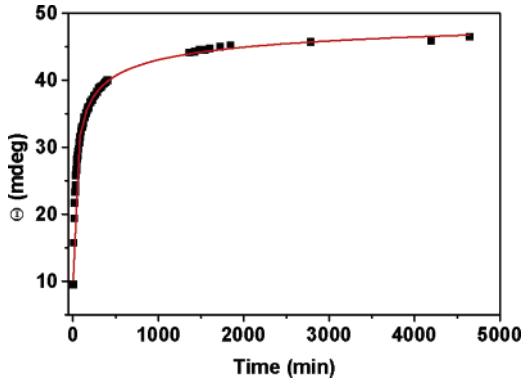

Figure 8. Time evolution of ellipticity at 264 nm for the [5′TGGGGT3′]$_4$ quadruplex assembly.

Table 3. Kinetic Parameters for Quadruplexes Association

quadruplex	N	k ($M^{-3}s^{-1}$)	$t_{1/2}$ (min)
[5′TGGGGT3′]$_4$	4	$(3.0 \pm 0.2) \times 10^7$	25 ± 1
[5′TGGGG3′-t]$_4$	4	$(2.1 \pm 0.1) \times 10^7$	35 ± 1
[t-5′GGGGT3′]$_4$	4	$(2.1 \pm 0.1) \times 10^7$	34 ± 1

quadruplex). The different results obtained by the SVD analysis when CD spectra are considered versus temperature (equilibrium melting experiments) and versus time (kinetic experiments) are not surprising. Indeed, these observations reflect the existence of kinetic, but not thermodynamic, intermediate species. Similar results were obtained by Lieberman and Hardin for the 5′TGGGG3′ sequence.[56] They found that, although quadruplex assembly is not a two-state process, the concentrations of intermediates become negligible asymptotically with reaction

Table 4. Results from Singular Value Decomposition of Quadruplex Kinetic Data

		autocorrelation	
quadruplex	singular values	U matrix	V matrix
[5′TGGGGT3′]$_4$	2562.731	0.9997	0.9792
	233.678	0.9996	0.8702
	22.603	0.9984	0.4175
	12.443	0.9946	−0.2111
	6.876	0.9739	0.5759
	5.336	0.9621	−0.0576
	5.269	0.9598	−0.0127
	4.697	0.9424	−0.2608
	4.404	0.9426	−0.0863
	4.298	0.9418	−0.0181
[5′TGGGG3′-t]$_4$	2475.236	0.9998	0.9797
	250.012	0.9995	0.9082
	42.978	0.9994	0.8201
	13.396	0.9881	−0.0985
	6.514	0.9781	0.5597
	4.590	0.9554	−0.3109
	4.430	0.9525	−0.3954
	4.223	0.9338	0.1133
	3.819	0.9335	−0.1585
	3.638	0.9323	−0.1219
[t-5′GGGGT3′]$_4$	2272.976	0.9997	0.9784
	240.976	0.9995	0.8924
	22.426	0.9942	0.6814
	18.832	0.9777	0.0907
	7.846	0.9523	−0.3980
	6.217	0.9571	−0.0320
	5.738	0.9534	0.2229
	5.233	0.9500	0.0768
	4.751	0.9428	−0.2660
	4.456	0.9394	−0.0078

time, which suggests the absence of thermodynamically stable intermediates. This could explain the absence of intermediate species when considering the dissociation/association process

(56) Lieberman, D. V.; Hardin, C. C. *Biochim. Biophys. Acta* **2004**, *1679*, 59−64.

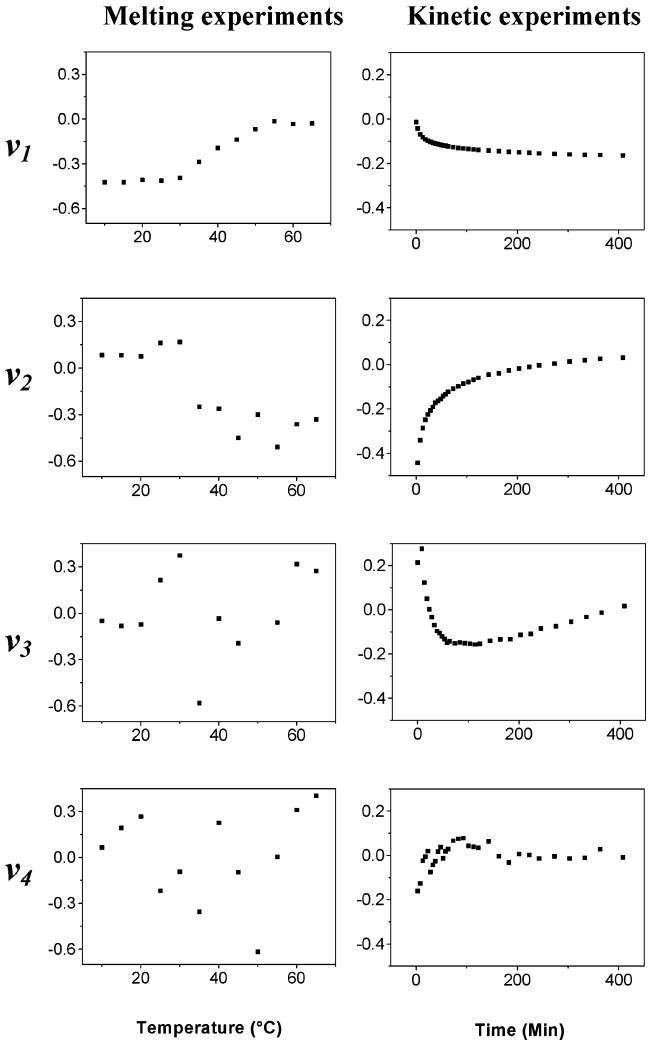

Figure 9. Comparison of the coefficient vectors v_1-v_4 from SVD analysis on the melting and kinetic CD spectra for the [$^{5'}$TGGGG$^{3'}$-t]$_4$ quadruplex.

at thermodynamic equilibrium. On the other hand, the experimental observation of the intermediate species only for the chimeric sequences suggests that the modified strands are able to form kinetically more stable dimers in comparison to the DNA strands in agreement with the slower kinetics observed for the association of the chimeric quadruplexes. In the absence of any structural data, we hypothesized that the dimers are represented by Hoogsteen G−G duplex that are half of the final quadruplex. In this frame the chimeric dimmers could be stabilized in comparison to the DNA counterpart by the lack of charge repulsion between the PNA units.

Conclusion

This study was aimed to explore the thermodynamic and kinetic properties of the chimeric quadruplexes [t-$^{5'}$GGGGT$^{3'}$]$_4$ and [$^{5'}$TGGGG$^{3'}$-t]$_4$ in comparison with their natural counterpart [$^{5'}$TGGGGT$^{3'}$]$_4$. Results from DSC and CD melting experiments show that modified quadruplexes are more stable than unmodified ones. SVD analysis suggests that the quadruplex melting, in equilibrium conditions, is a two-state process for all the studied systems. This result is consistent with the close correspondence observed between the calorimetric and van't Hoff enthalpies. Inspection of the thermodynamic parameters indicates that only the 5′-PNA units give an effective enthalpic contribution to quadruplex stabilization. Molecular dynamic studies can explain this result by suggesting the formation of two stable intrastrand T−T base pairs between the thymines of the 5′-PNA units, whereas an opening of the 3′-PNA units was observed on a nanosecond time scale. Further, the chimeric strands show slower association kinetics in comparison to the unmodified ones. A two-sequential association mechanism was invoked to interpret the fourth-order behavior of the association kinetics. The SVD analysis on the CD kinetic data reveals the presence of a kinetically stable intermediate species in the association process of the chimeric quadruplexes, but no intermediate species was detected for the DNA quadruplex.

Our study on chimeric quadruplexes extends the repertoire of quadruplex forming oligonucleotides which can be utilized as potential aptamers, or nonantisense agents. We show that the incorporation of a PNA unit into oligonucleotides affects their folding and produces useful changes in biophysical properties of the resulting quadruplexes. Particularly, the knowledge of the energetic parameters inherent to quadruplex formation is crucial in view of their applications as therapeutic agents. It is evident, in fact, that both kinetic and thermodynamic factors may be important in physiological conditions. In the future, it is desirable to investigate stability−activity relationships for the selection of nucleic acid biotargets or to improve the design of novel aptameric nucleic acids with better molecular recognition abilities with respect to native DNA sequences.

Acknowledgment. This work was supported by a PRIN-MURST grant 2002−2003 "Sintesi e caratterizzazione chimico-fisica di triple e quadruple eliche di DNA di interesse biologico e farmacologico" from the Italian "Ministero dell'Università e della Ricerca Scientifica e Tecnologica" (Rome) and by "Centro Regionale di Competenza per l'Analisi e il Monitoraggio del Rischio Ambientale (AMRA)".

Supporting Information Available: Apparent molar heat capacity vs temperature profiles (Figure S1). CD spectra vs time for the three quadruplex formation (Figure S2) and complete ref 48. This material is available free of charge via the Internet at http://pubs.acs.org.

JA0545923